E-ISSN: 2706-8927
P-ISSN: 2706-8919
www.allstudyjournal.com
IJAAS 2020; 2(4): 10-13
Received: 06-08-2020
Accepted: 11-09-2020

Anshu Kumari
Former, Research Scholar, Department of Physics, LNMU, Darbhanga, Bihar, India

Corresponding Author:
Anshu Kumari
Former, Research Scholar, Department of Physics, LNMU, Darbhanga, Bihar, India

Study of the resonance coupling in plasmonic nanomatryoshka homo and heterodimers

Anshu Kumari

Abstract
We propose a method to analyze the behavior of multilayer concentric nanoshell particles in an antisymmetric orientation employing full dielectric function calculations and the Drude model based on interband transitions in metallic components. This study provides a method to predict the behavior of the higher energy plasmon resonant modes in entirely antisymmetric structures such as compositional heterodimers.

Keywords: Resonance Coupling, Plasmonic Nanomatryoshka Homo and Heterodimers

Introductions
Metallic nanostructures with subwavelength dimensions have been extensively employed in the design and fabrication of integrated nanoplasmonic structures and devices for numerous applications such as biological and chemical sensing, and surface-enhanced Raman spectroscopy (SERS). Studies have strongly proved that various parameters such as shape, geometrical dimensions, chemical composition, and optical characteristics of the nanostructures have a significant impact on intensity, position, and frequency of the plasmon resonant modes [1–4].
In addition, the behavior of plasmon resonances strongly depends on the existence of an adjacent individual nanoparticle. Subtle variations in the elucidated chemical, physical, and optical properties influence the plasmon resonance condition due to the near-field coupling of dipoles, quadrupoles, and higher-order poles under the excitation of an incident beam. Coupling of plasmon resonances to proximal nanoparticles facilitates an opportunity to adjust the intensity of the LSPR at the desired spectrum via red- or blue-shifts. Moreover, by changing the distance between nanoparticles, scattering cross-section spectra can be tuned, which can be exploited for imaging and sensing purposes.

Analysis
To improve the quality of designed plasmonic devices, all alterations must be performed correctly and accurately. For instance, it is well accepted that increments in the refractive index of the local environment cause red-shift of the plasmon resonance frequency to the longer wavelength spectra. More studies have also shown that this sensitivity of the plasmon resonance frequency can be improved by changing the shape and size of the nanoparticles simultaneously in the correct manner. Considering the dipolar coupling, and Drude model, the nanoparticle geometry-dependent factor (shape factor) as κ, and the refractive index of host substance by n_h, we can describe the precise surface plasmon wavelength as:

$$\lambda_{SP} = \sqrt{\frac{\varepsilon_0 m_e(\varepsilon_\infty + \kappa n_h^2)}{Ne^2}} \quad (1)$$

where, N is the electron density of the employed metal, ε_0 and ε_∞ are the permittivity of free space and high-frequency response respectively, and me is the effective electron mass.
In contrast, in the heterodimer regime (out-of-phase mode), the adjacent heterodimer shows the antibonding modes as well as bonding modes resulting localized electric field enhancement at the outer sides of the dimer configurations and blue-shift of the plasmon resonance frequency, which is denoted by σ*. Both bonding and antibonding plasmon modes and their hybridized models are explained in the following sections.

The plasmon response of the proposed nanostructures with expected red- and blue-shifts are also examined theoretically and numerically. Moreover, the effect of changes in the polarization direction and plasmon resonance reflection in both in-phase and out-of-phase plasmon modes are of interest for this study. Earlier works have shown that modifications in the polarization direction of an incident wave to the transverse polarized mode (perpendicular to the dimer axis) leads to an exactly opposite results in the shift of the plasmon resonant modes and it is important to note that corresponding shifts of the LSPR are noticeably weaker than the former case. In this limit, an antibonding mode is reported for the homodimer structure, while a bonding mode is observed for the heterodimer structure which are denoted by π and π*, respectively.

In this work, we investigate the plasmon response and optical properties of plasmonic nanostructures composed of two concentric nanoshells that are placed in close proximity to each other and are known as NM dimers. The in-phase regime of NM dimer have already been studied by Prodan et al.6 and the behavior of bonding modes are examined previously. In the antisymmetric regime, we show that the proposed dimer is able to support both bonding and antibonding plasmon modes, concurrently. Most of the previous investigations were limited to dimers with ordinary shapes or materials with similar compositions. In this report, we extend our study to the NM structure with different metal compositions and sizes. This method allows us investigating the plasmon resonance behavior in symmetry-lacking structures. Moreover, we examine the quality of the plasmon resonance coupling in the NM structures with various geometrical dimensions to achieve enhanced and ultra-sensitive nanoplasmonic configurations.

Results and discussion

We examine the quality of bonding and antibonding plasmon resonance modes for a NM homodimer (symmetric (Ψ_1+Ψ_2)) with the same geometrical parameters and metal compositions (gold) for both sides, while the separation or gap distance between NM units is approximately D_{in}~15 nm, which resembles the strong coupling regime and also the thickness of the rings is kept fix as 25 nm throughout the study. This examination helps us observe bonding and antibonding plasmon modes in heterostructures under illumination of incident polarized light.

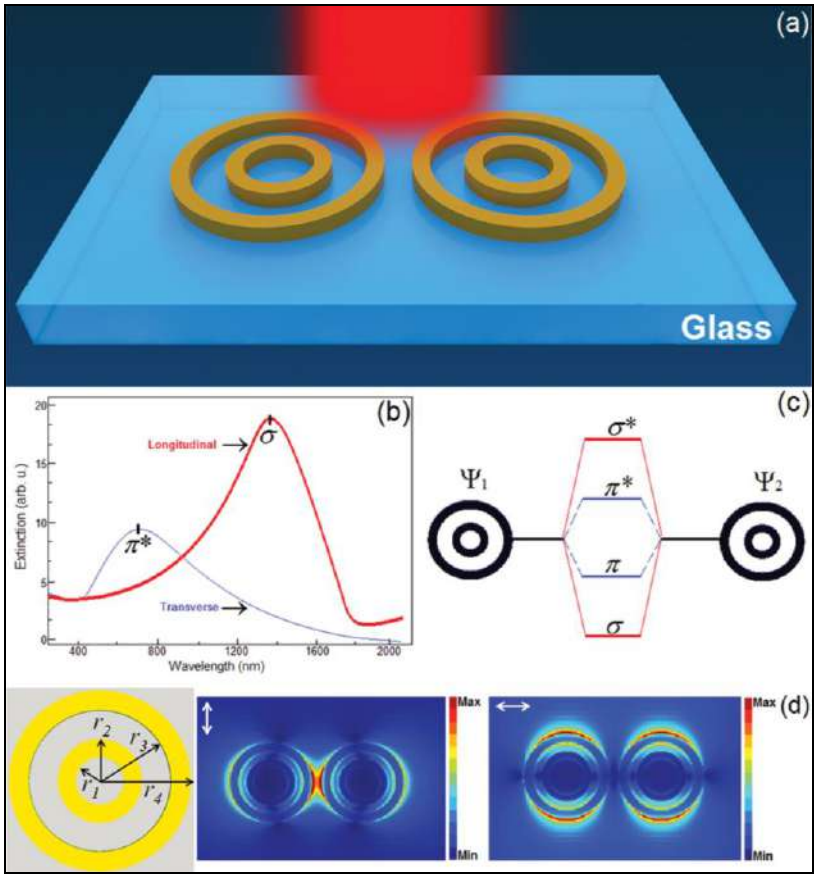

Fig 1: shows a three-dimensional schematic picture of a symmetric homodimer, along with the geometrical parameters in the top-view picture

FIG. 1. (a) Schematic diagram of a gold NM homodimer (Ψ1+Ψ2). (b) The extinction cross-section spectrum for both longitudinal (σ) and transverse (π*) modes, which correspond to the bonding plasmon modes, according to the plasmon hybridization model. (c) Energy level diagram for plasmon hybridization homodimer in transverse and longitudinal polarizations excitations. (d) The E-field maps for the plasmon resonance excitation in the homodimer system under longitudinal and transverse polarized beams. The effective geometrical parameters (radii) which play a fundamental role in the investigation of the nanostructure and LSPR behavior, are also shown. These parameters are the same for both nanoparticles and are (r_1, r_2, r_3, r_4) = (60, 80, 105, 135) nm. The thickness for all cases is 25 nm.

Figure 1(a) shows a three-dimensional schematic picture of a symmetric homodimer, along with the geometrical

parameters in the top-view picture (not to scale). It is already proved that the interaction of surface plasmon polaritons (SPPs) in the interior and exterior surfaces of a nanoshell can be described by the plasmon hybridization theory, and the corresponding frequency for antisymmetric and symmetric modes can be specified by $|\omega_+\rangle$ and $|\omega_-\rangle$, respectively. Figure 1(b) illustrates the extinction cross-section profile for the observed plasmon resonant modes under excitation of longitudinal and transverse electric field polarization modes in strong coupling regime. Obviously, the two bonding plasmon modes result from the longitudinal (σ) (larger shift) and transverse (π*) polarization modes with the extinction peaks at λ*1390nm and 780nm, respectively. Figure 1(d) shows the plasmon resonance excitation as E-field maps for the homodimer antenna. One should note that these results have been predicted from the plasmon hybridization model for most of the comparable and simple homodimers with short red-shifts under the excitation by an incident longitudinally polarized light.7–8 Considering the geometrical dimensions (r_1,r_2,r_3,r_4) = (60,80,105,135) nm for gold NM, we calculated the extinction spectra for the homodimer system in the strong interaction of the excited dipolar and multipolar fields (bonding modes only). Further, we evaluated the plasmon resonance behavior (coupling and shifting of the LSPR) during symmetry breaking for the NM dimer based on modifications in the geometrical sizes, while the chemical properties of the employed materials are the same in both sides. Accordingly, we modified

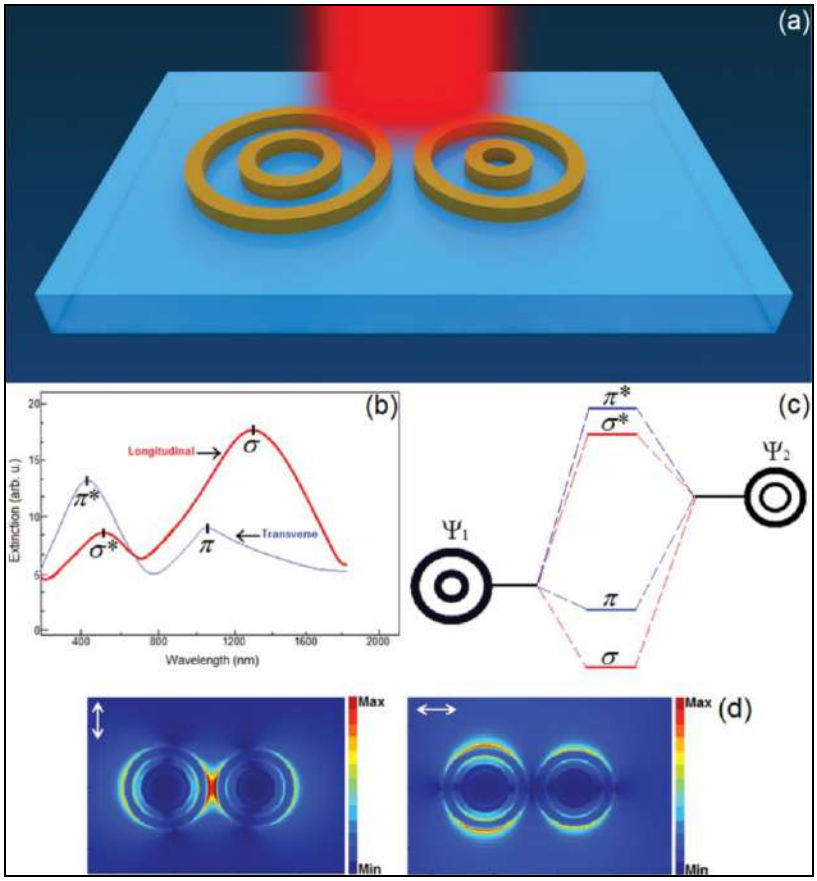

Fig 2: Two distinct extremes induced for each one of the incident polarized modes in the symmetry breaking regime

FIG. 2. (a) Schematic diagram of a gold antisymmetric dimer (Ψ_1 +Ψ_2) with the modified geometrical dimensions of (60, 80, 105, 135) nm for Ψ_1 and (50, 65, 95, 125) nm for Ψ_2. (b) The extinction cross-section spectra for both of the longitudinal and transverse polarization. The LSPR shows a trivial blue shift in the σ mode and also for the π*-mode due to the coupling of plasmon modes. Hence, the extinction maximums are at λ*1360, 510 nm and 1080, 470 nm for (σ,σ*) and (π,π*), respectively. (c) Plasmon hybridization diagram for the proposed NM heterodimer in the transverse and longitudinal polarizations. (d) The E-field maps for the plasmon resonance excitation in the homodimer system under longitudinal and transverse polarized beams.

the radii of one of the gold NM units (Ψ_1) to (50,65,95,125) nm, while keeping the ones for the other (Ψ_2) at (60,80,105,135)nm (Heterodimer antenna, see Fig. 2(a)). The corresponding extinction cross-sectional profile is illustrated in Fig. 2(b), where two distinct extremes induced for each one of the incident polarized modes in the symmetry breaking regime. The incident longitudinal polarization excites the peaks at λ*1360nm (σ), 510nm (σ*) while the incident transverse polarization results the extremes at λ*1080nm (π), 470nm (π*) for bonding and antibonding plasmon modes in the antisymmetric regime (Ψ_1-Ψ_2), respectively. Utilizing the coupled dipole-dipole model and discrete approximation (DDA) method,9–10 for the multipolar modes, we calculated the energy diagram for different regimes as shown in Fig. 2(c). It is shown that DDA method is a highly flexible analytical method for computing the spectral responses and corresponding extinction profiles of nanoscale structures.11 Considering the proposed method in Ref. 27, therefore, the extinction cross-section for a NM unit can be written as:

$$C_{ext} = \frac{4\pi k}{|E_0|^2} \sum_{i=1}^{2} \mathrm{Im}\left(E^*_{inc,j}.P_j\right) \quad (2)$$

where k is the wave vector, E_{inc} is the incident electric field, p is the dipole moment depending on the polarizability of NM unit and dipolar field. The polarizability and spectral response of a plasmonic NM is calculated and discussed in previous studies comprehensively. Using previously studied analysis, we extracted the plasmonic responses for both homo and heterodimers accurately. Considering the same chemical properties of plasmonic NM units, it is obvious that the antibonding mode as an abnormal mode repeals the excited dipoles of the small and large gold concentric nanoshells. These results encouraged us to develop a modified version of computations for analyzing the behavior of a dimer structure composed of two different NM units that will be discussed further. We plotted the E-field maps for the plasmon resonance hybridization in the gap spots between nanoparticle units for bonding modes (σ and π) positions in Fig. 2(d).

Conclusions

We making changes in the physical dimensions and chemical compositions (silver-gold) of the utilized NM units showed a plasmon coupling and an interband absorption corresponding to the gold nanoshells. This led to an abnormal red-shift of higher energy modes (σ* and π*), which caused by coupling between interband absorption of gold shells and plasmon resonance of silver shells. Such a shift of LSPR is not expected by the plasmon hybridization model. Utilizing a modified hybridization model based on full dielectric function computations and the Drude model which have previously used for nanospheres and extended to multilayer shells, we obtained an expected blue-shift of plasmon resonance for higher energies. The variation of the optical response and plasmon resonance which caused by subtle structural and compositional alterations could transmute the modified nanostructures into a multipurpose scheme for LSPR sensing applications.

References

1. Elghanian R, Storhoff JJ, Mucic RC, Letsinger RL, Mirkin CA. Selective colorimetric detection of polynucleotides based on the distance-dependent optical properties of gold nanoparticles, Science 277, 1078-1081 (1997). 065102-9 Ahmadivand, Sinha, and Pala AIP Advances 6, 065102, 2016.
2. Nie S, Emory SR. Probing single molecules and single nanoparticles by surface-enhanced Raman scattering, Science 1997;275:1102-1106.
3. Kelly KL, Coronado E, Zhao LL, Schatz GC. The optical properties of metal nanoparticles: The influence of size, shape, and dielectric environment, J Phys Chem B 2003;107:668-677.
4. Jain PK, Huang X, El-Sayed IH, El-Sayed MA. Noble metals on the nanoscale: Optical and photothermalproperties and some applications in imaging, sensing, biology, and medicine, Acc Chem Res 2008;41:1578-1586.
5. Prodan E, Radloff C, Halas NJ, Nordlander P. A hybridization model for the plasmon resonance of complex nanostructures, Science 2003;302:419-422.
6. Ahmadivand A, Karabiyik M, Pala N. Fano-like resonances in split concentric nanoshell dimers in designing negative-index metamaterials for biological-chemical sensing and spectroscopic purposes, Appl Spectrosc 2015;69:563-573.
7. Sheikholeslami S, Jun YW, Jain PK, Alivisatos AP. Coupling of optical resonances in a compositionally asymmetric plasmonic nanoparticle dimer, Nano Lett 2010;10:2655-2660.
8. Taubenblatt MA, Tran TK. Calculating of light scattering from particles and structures on a surface by the coupled-dipole method, J Opt Soc Am A 1993;10:912-919.
9. Draine BT, Flatau PJ. Discrete-dipole approximation for scattering calculations, J Opt Soc Am A 1994;11:1491-1499.
10. Bohren CF, Huffman DR. Absorption and scattering of light by small particles Wiley, Germany, Berlin 1983.
11. Logsdail AJ. Computational characterization of gold nanocluster structures Springer, Switzerland 2013.